Neuroimaging of Vascular Autoregulation by fDOT: A Modeling Study

Yong Xu[1,2], Yaling Pei[2], Harry L. Graber[1,2], and Randall L. Barbour[1,2]

[1]Dept. of Pathology / SUNY Downstate Medical Center / 450 Clarkson Ave. Brooklyn, NY 11203; yong.xu@downstate.edu

[2]NIRx Medical Technologies LLC / 15 Cherry Lane / Glen Head, NY 11545

INTRODUCTION

As a technique for noninvasive monitoring of biomedical function, diffuse optical tomography (DOT) offers a number of practical, economic, and physiologic informational advantages relative to other imaging modalities [1,2]. The technology is compact, can be brought to the bedside, and is easily combined with other imaging technologies. In addition, by extending the measurement to allow for the capture of a time series, it can explore various dynamic phenomena, in particular, those associated with the hemoglobin signal [3-5].

An especially important class of dynamic phenomena are those tied to feedback mechanisms which serve to regulate a multitude of biological processes. Among these is vascular autoregulation, which is the process by which tissues self-regulate their blood supply in response to varying metabolic demand. In this and accompanying series of reports (219 M-AM, 229 M-AM, 222 M-PM, 145 W-AM), we explore the hypothesis that by using appropriate data sampling and analysis approaches, we can delineate features associated with autoregulatory processes in much greater detail than previously appreciated.

To systematically document this, here we have applied modeling techniques to study the fidelity by which autoregulatory transitions in a head model can be recovered using optode configurations similar to that used in clinical studies.

METHODS

• FEM Model and Optode Configurations:

Figure 1A shows a FEM mesh employed together with the possible optode positions. Two meshes were used in this report. One is a fine mesh with 5274 nodes and 26,119 elements, used for simulated measurement generation. The other is a coarse mesh that has 2620 nodes and 11363 elements for inverse calculations. Three optode configurations were investigated, as shown in Figure 1Cs. C1 has 30 sources and 30 detectors; C2 has 22 sources and detectors; and C3 is 15 sources and detectors.

• Optical Properties and Hemodynamic States:

Modeled is a weakly absorbing homogeneous scattering medium (μ_a = 0.055-.070/cm, μ_s = 10/cm) containing two regions 1.5 cm in diameter, separated by 2.5 cm and whose center is ~1.5 cm below the surface (Figure 1B). As shown in Figure 2A, also modeled are time variations in the absorption properties of these regions that correspond to the changes in Hb levels of a magnitude typically seen in the cortex (~30%). Figure 2B shows the accompanying variations in Hb autoregulatory states in the modeled inclusions.

• Forward Solutions:

Simulated detector readings for a specific optode configuration were acquired by using the finite element method to solve the diffusion equation, with a DC source term and Robin boundary conditions, as described in Ref. [5].

• Inverse Solutions:

Images were reconstructed by using the previously described Normalized Difference Method (NDM) [6], which is a modified linear perturbation technique that is highly robust to many difficult-to-eliminate sources of experimental error and uncertainty associated with DOT measurements.

• Detector Noise Models:

Noise-free detector data were used in the first instance, and Gaussian white noise was added to the normalized detector data in the rest. As in previous reports, here we used a noise model in which, for each source-detector channel, the noise level (i.e., the standard deviation of the noise distribution) is a pre-selected percentage of the noise-free detector reading and grows as the fourth power of the distance between source and detector [7]. In the five noise-added trials, the minimal noise level (source and detector co-located) was 1, 2 , 3, 5, or 8%, while the maximal noise level was, respectively, 10, 20, 30, 50 or 80%, which are defined as the noise levels 1,2,3,5, and 8 (used in Figure 6 and Table 2 and 3). The noise distributions used for each trial were stationary, i.e., the noise levels were not time-varying.

• Noise Suppression for Recovered Images:

Reconstructed images recovered from noisy detector data were subsequently treated with two noise-suppression schemes. The first method was temporal low-pass filtering (tLPF) with a zero-phase FIR digital filter, using a trapezoidal frequency-response function with threshold frequency set to 0.15 Hz and a 0.05 Hz roll-off. The second noise-suppression scheme was spatial "pillbox" filtering (sLPF), wherein the image value at each FEM node is replaced by a weighted average of the values at that node and its near neighbors [7].

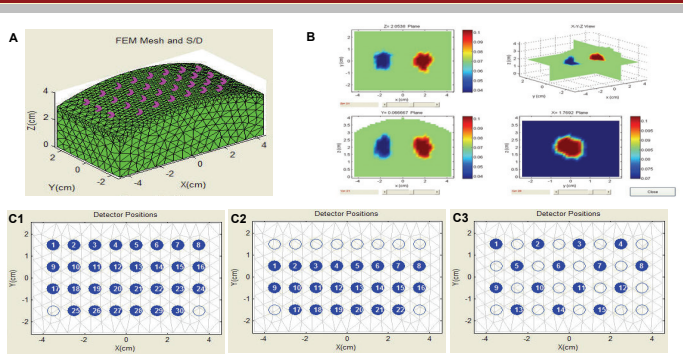

Figure 1. Panel A. FEM mesh with indicated optode positions. Mesh: (Nodes) 2620, (Elements) 11363. Panel B. Orthogonal views of medium with 1.5 cm diameter inclusions. Panel C. Three optode configurations. C1: 30x30 channels; C2: 22x22 channels; C3: 15x15 channels.

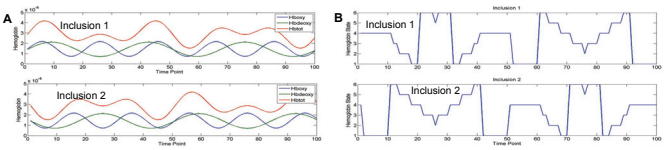

Figure 2. Panel A: Dynamics of Hb response for left (inclusion 1) and right (inclusion 2) inclusions shown in Figure 1B. Panel B: Corresponding autoregulatory states for two inclusions.

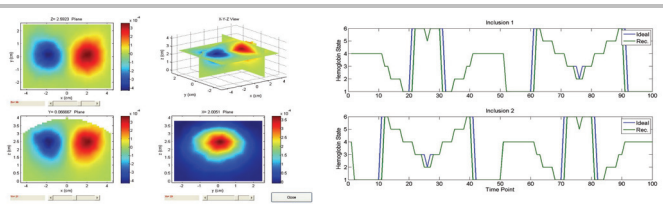

Figure 3. Reconstructed images and autoregulatory states from nose-free simulated data for optode configuration C1 (30x30 channels) . Left Panel: Absorption images at time point 45. Right Panel: Autoregulatory states for two inclusions.

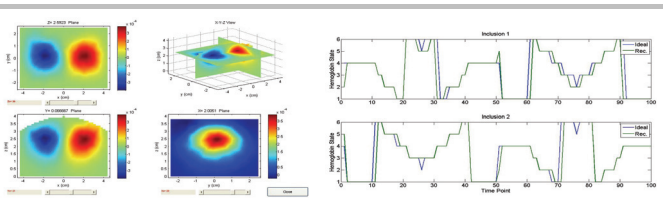

A. Noise level: 1%-10%

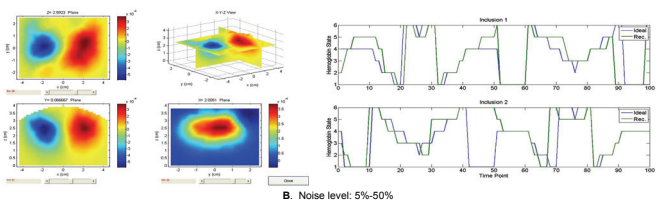

B. Noise level: 5%-50%

Figure 4. Reconstructed absorption images and autoregulatory states from noisy simulated data for optode configuration C1 (30x30 channels) . Panel A: for noise level (1%--10%). Panel B: for noise level (5%--50%).

RESULTS

Qualitative and quantitative assessments of the fidelity of our method is presented in Figures 3-6 and Table 2 and 3. Shown in Figures 3 and 4 are reconstruction results without and with added noise, respectively. As detailed in Figure 5, image accuracy, as defined by the fraction of the total time series the correct autoregulatory state is recovered, declines linearly with increasing noise. This rate is increased modestly by using more sparse illumination detection conditions. In all, acceptable recovery accuracy is maintained when noise is limited to the 2-20% range.

Shown in Tables 2 and 3 is the dependence of image quality on depth of the inclusion with different array conditions (C1, C3). Here we estimated this by fractionating the inclusion into two regions; one located near top and the other near the bottom aspect of the inclusion; ~1.0 and 2.2 cm from the surface). Inspection shows that good accuracy (~80%) is retained for noise level ≤ level 2 for inclusion depths of to 2.2 cm. With more sparse illumination conditions, nearly equivalent performance is limited to noise level 1.

Results in Figure 6 show the spatial extent of recovery of the autoregulatory states as a function of noise level for the C1 measurement configuration. Images shown were thresholded in accordance to the expected greater temporal variance for pixels containing the inclusion (normalized CV > 50%). Inspection shows that only nominal degradation in image quality occurs for noise ≤ level 2.

CONCLUSIONS

1. Recovery accuracy of >80% is retained in most cases for noise conditions up to level 2. Higher noise levels or use of more sparse measurement conditions causes more rapid degradation of image quality.
2. Overall performance using typical noise levels seen in experimental studies indicates that good recovery of the hemoglobin autoregulatory states is feasible.

REFERENCES

[1] R.L. Barbour, H.L. Graber, Y. Pei, S. Zhong, C.H. Schmitz, "Optical tomographic imaging of dynamic features of dense-scattering media," *J. Optical Society of America A*, Vol. 18, pp. 3018-3036 (2001).

[2] G. S. Landis, T. F. Panetta, S. B. Blattman, H. L. Graber, Y. Pei, C. H. Schmitz, R. L. Barbour, "Clinical applications of dynamic optical tomography in vascular disease," in *Optical Tomography and Spectroscopy of Tissue IV (Proceedings of SPIE, Vol. 4250)*, B. Chance, R. R. Alfano, B. J. Tromberg, M. Tamura, E. M. Sevick-Muraca, Eds., pp. 130-141 (2001).

[3] C.H. Schmitz, H.L. Graber, Y. Pei, M.B. Farber, M. Stewart, R.D. Levina, M.B. Levin, Y. Xu, R.L. Barbour, "Dynamic studies of small animals with a four-color DOT imager," *Review of Scientific Instruments*, Vol. 76, 094302 (2005).

[4] C.H. Schmitz, D.P. Klemer, R.E. Hardin, M.S. Katz, Y. Pei, H.L. Graber, M.B. Levin, R.D. Levina, N.A. Franco, W.B. Solomon, R.L. Barbour, "Design and implementation of dynamic near-infrared optical tomographic imaging instrumentation for simultaneous dual-breast measurements," *Applied Optics*, Vol. 44, pp. 2140-2153 (2005).

[5] H.L. Graber, Y. Pei, R.L. Barbour, "Imaging of spatiotemporal coincident states by DC optical tomography," *IEEE Transactions on Medical Imaging*, Vol. 21, pp. 852-866 (2002).

[6] Y. Pei, H.L. Graber, R.L. Barbour, "Influence of systematic errors in reference states on image quality and on stability of derived information for DC optical imaging," *Applied Optics*, Vol. 40, pp. 5755-5769 (2001).

[7] Y. Xu, Y. Pei, H.L. Graber, R.L. Barbour, "Image quality improvement via spatial deconvolution in optical tomography: Time-series imaging," *J. Biomedical Optics*, Vol. 10, 051701 (2005).

ACKNOWLEDGMENTS

Funded by the National Institute of Neurological Disorders and Stroke (R41 NS050007-01).

Hemoglobin State	State 1	State 2	State 3	State 4	State 5	State 6
Hb_{oxy}	-	-	-	+	+	+
Hb_{deoxy}	-	+	+	+	-	-
Hb_{tot}	-	-	+	+	+	-
	Balanced	Uncomp. oxygen debt	Comp. oxygen debt	Balanced	Uncomp. oxygen excess	Comp. oxygen excess

Table 1. Hb states paired according to Hb dependence on autoregulation.

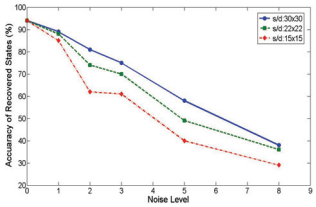

Figure 5 . Dependence of recovery accuracy with noise level and optode configurations.

	Noise Level 0	Noise Level 1	Noise Level 2	Noise Level 3	Noise Level 5
Z=3 (cm)	94	88	80	73	68
Z=2 (cm)	94	84	73	64	42

Table 2 . Dependence of recovery accuracy (%) with pixel depths for optode configuration C1 (30x30 channels) .

	Noise Level 0	Noise Level 1	Noise Level 2	Noise Level 3	Noise Level 5
Z=3 (cm)	94	85	68	63	55
Z=2 (cm)	94	80	49	51	27

Table 3 . Dependence of recovery accuracy (%) with pixel depths for optode configuration C3 (15x15 channels) .

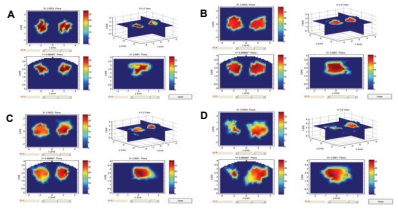

Figure 6. Recovered autoregulatory state 1 images for optode configuration C1 . Panels A: no noise; B: noise level 1; C: noise level 2; D: noise level 3.